

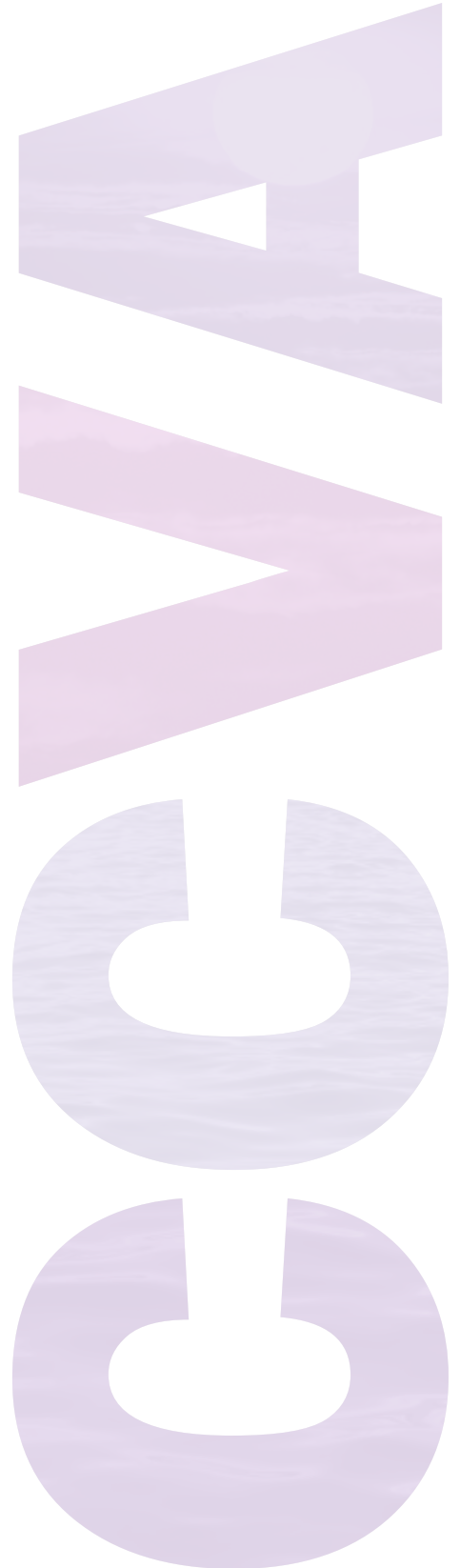
# Appendix D

## Urban Heat Island Protocol for Mapping Temperature Projections

**Climate Change Vulnerability Assessment**

**City of Cambridge, Massachusetts**

November 2015



# Acknowledgements

## City of Cambridge

Richard C. Rossi, City Manager

Lisa C. Peterson, Deputy City Manager

## Project Steering Committee

John Bolduc, Environmental Planner, Community Development Department, Project manager

Iram Farooq, Assistant City Manager for Community Development

Sam Lipson, Environmental Health Director, Public Health Department

Brian Murphy, Assistant City Manager for Community Development

Owen O'Riordan, Commissioner of Public Works

Susanne Rasmussen, Environmental & Transportation Planning Director, Community  
Development Department

Kathy Watkins, City Engineer, Department of Public Works

## Produced in Collaboration with

Kleinfelder, Lead Consultant

Nathalie Beauvais, Project Manager

Lisa Dickson, Principal in Charge

Indrani Ghosh, Technical Lead

Anthony Wohletz, Heat Modeling

Andrew Nunnery, Climate Data Analysis

Karin Hagan, GIS Lead

Vijay Kesavan, Vulnerability Assessment, GIS

For more information on the project, please visit the City website at

<http://www.cambridgema.gov/climateprep>

## Table of Contents

Background on Thermal Remote Sensing .....	1
Overview of Methodology .....	2
Selecting Satellite Data .....	3
Converting Thermal Data to Radiance .....	6
Estimating Emissivity .....	6
Estimating Atmospheric Distortion.....	10
Calculating Emissivity- and Atmosphere-corrected Land Surface Temperature .....	13
Estimating Ambient Air Temperature.....	16
Calculating Heat Index.....	17
Estimating the Cooling Impact of Vegetation.....	20
Future Conditions.....	24
References .....	29

## List of Figures, Equations, and Schematics

### *Figures*

- Figure 1: Process for mapping heat index
- Figure 2: Historical temperature data
- Figure 3: Image availability, 2010
- Figure 4: Estimated existing ambient air temperature
- Figure 5: Relative humidity vs temperature
- Figure 6: Estimated existing heat index
- Figure 7: Existing tree canopy
- Figure 8: Temperature vs. tree canopy regression
- Figure 9: Mapping estimated cooling impact of tree canopy
- Figure 10: Estimated future conditions ambient air temperature variability for 2030s
- Figure 11: Estimated future conditions ambient air temperature variability for 2070s
- Figure 12: Future conditions heat index variability for 2030s
- Figure 13: Future conditions heat index variability for 2070s

### *Equations*

- Equation 1: Calculating thermal at-satellite spectral radiance
- Equation 2: Calculating VIR and NIR at-satellite spectral radiance
- Equation 3: Calculating VIR and NIR atmosphere-corrected radiance
- Equation 4: Calculating  $L_p$  for equation 3
- Equation 5: Calculating L1% for equation 4
- Equation 6: Calculating NDVI from NIR and VIT atmospherically-corrected reflectance
  
- Equation 7: Estimating emissivity from NDVI
- Equation 8: Calculating soil/vegetation-mixture emissivity for equation 7
  
- Equation 9: Calculating  $P_v$  for Equation 8
- Equation 10: Estimating land surface radiance via a simplified radiative equation
  
- Equation 11: Planck's Function: spectral intensity from wavelength and temperature
  
- Equation 12: Inverting Planck's Function
- Equation 13: Landsat 5 brightness temperature equation
- Equation 14: Average ambient air vs land surface temperature ratio
- Equation 15: Estimating relative humidity from ambient air temperature
- Equation 16: Calculating heat index
- Equation 17: Calculating heat index where heat index is less than 80
- Equation 18: Temperature vs. tree canopy regression
- Equation 19: Estimating cooling impact of tree canopy
- Equation 20: Future conditions ambient air temperature for 2030
- Equation 21: Future conditions ambient air temperature for 2070
- Equation 22: Future conditions heat index for 2030
- Equation 23: Future conditions heat index for 2070

### *Schematics*

- Schematic 1: NASA Online MODTRAN Tool

## Background on Thermal Remote Sensing

Creating a high-resolution temperature map is a challenge considering that there is a limited number of temperature stations to estimate average temperature over most parts of an urban area.

Satellite data offer a proxy through *thermal remote sensing* where the temperature of surfaces depicted in satellite images is calculated from satellite data. Thermal remote sensing works by calculating *brightness temperature*. All objects emit radiation. According to Planck's law, the spectral intensity of radiation is related to the temperature of the object and radiation wavelength. Given spectral intensity and the wavelength of radiation, the temperature of the object emitting radiation can be calculated. This is known as the brightness temperature.

Satellites record a series of images over different spectral ranges, or *bands*. Most bands focus on radiation emitted by the sun and reflected back to space by objects on Earth. These bands cover *visible light*. But not all this sun-emitted radiation is reflected back to space. Earth absorbs some of this radiation, and in response emits its own radiation. In a concept known as *energy balance*, Earth warms until the energy it emits equals the energy it absorbs. The energy Earth emits is almost entirely within longer wavelength bands than the energy the sun emits. Earth's spectral range is referred to as *thermal radiation* or *infrared radiation*.

Infrared bands recorded by satellites capture the radiation emitted by the Earth. Data embedded in the images, *digital numbers*, are directly proportional to radiance, which is a measurement of spectral intensity. When analyzed on their own, digital numbers can be used to understand *relative temperature distribution*. Because the average wavelength of the infrared band is known, radiance and wavelength can therefore be used to calculate brightness temperature. When calculated from satellite data, brightness temperature is typically known as *at-satellite temperature*. When corrected for atmospheric distortion and land surface emissivity variance, at-satellite temperature provides an estimate of *land surface temperature*. And when adjusted for typical differences between the land surface temperature and air temperature, land surface temperature provides an estimation of *ambient air temperature*.

## Overview of Methodology

Landsat 5 satellite imagery was selected for analysis based on review of historical temperature and image availability. Thermal digital numbers were converted to at-satellite radiance (equation 1). At-satellite radiance can be converted directly to at-satellite temperature (equation 11); however, at-satellite radiance was first corrected for emissivity and atmospheric distortion. Emissivity was estimated (equations 7, 8, and 9) from NDVI (equations 2, 3, 4, 5, and 6). Atmospheric parameters were estimated using the NASA online MODTRAN tool (schematic 1). Land surface radiance was then calculated (equation 11) using emissivity and atmospheric estimates, and land surface radiance was used to estimate land surface temperature from the inverted Planck's Function (equation 12) for Landsat 5 (equation 13). Ambient air temperature was estimated (equation 14) by scaling average land surface temperature to average ambient air temperature. Relative humidity was estimated based on a linear regression model relating relative humidity to temperature (equation 15), and heat index was calculated based on the standard NOAA regression (equation 16). Ambient air temperature was compared with tree canopy percentage (Figure 8) and the cooling impact of vegetation was estimated (equation 19).

The process is illustrated in Figure 1 and presents a nine-step approach:

1. Selecting satellite data
2. Converting thermal data to radiance
3. Estimating emissivity
4. Estimating atmospheric distortion
5. Calculating emissivity- and atmospheric-distortion-corrected land surface temperature
6. Estimating ambient air temperature
7. Estimating heat index
8. Estimating the cooling impact of vegetation
9. Estimating future conditions

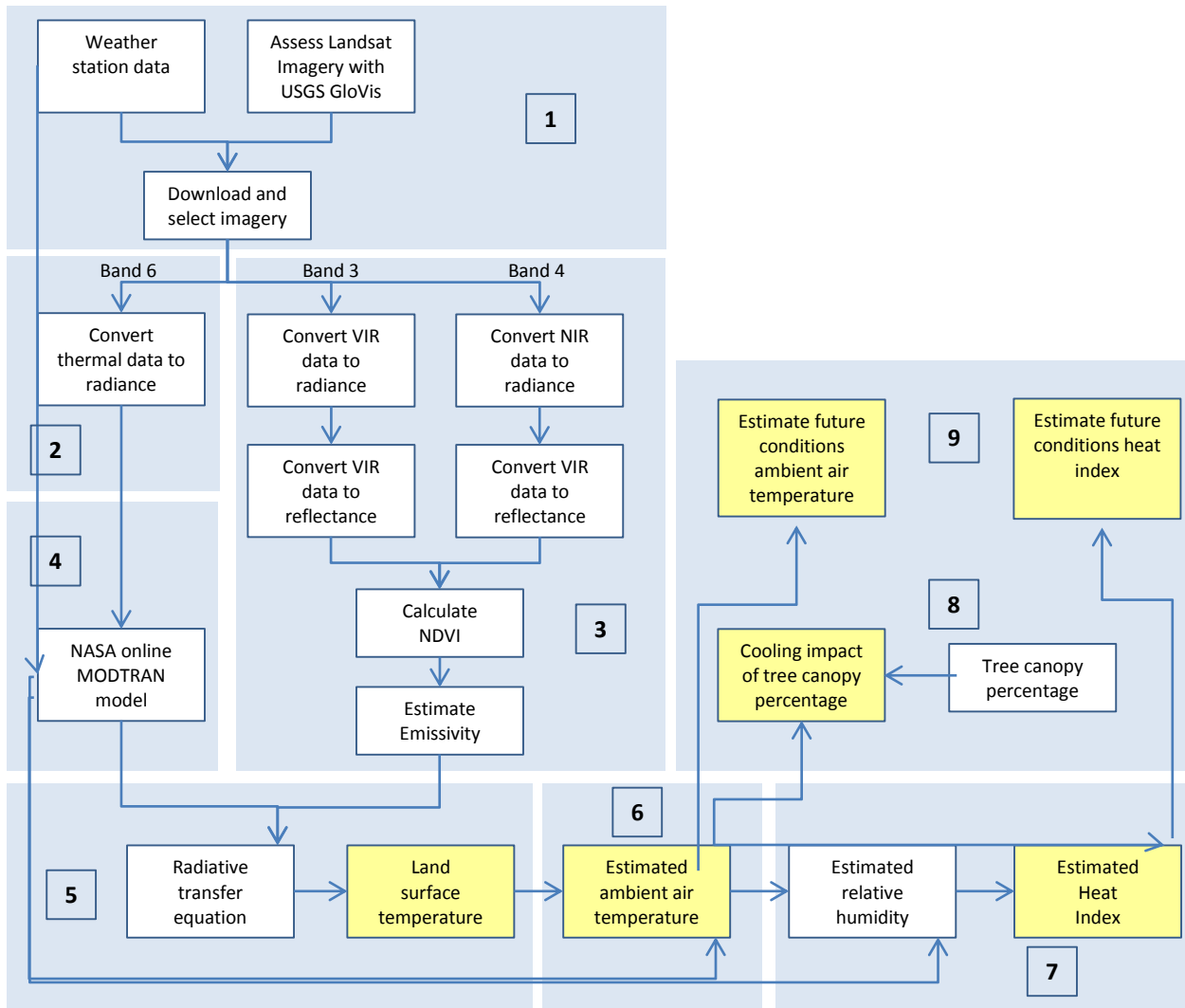


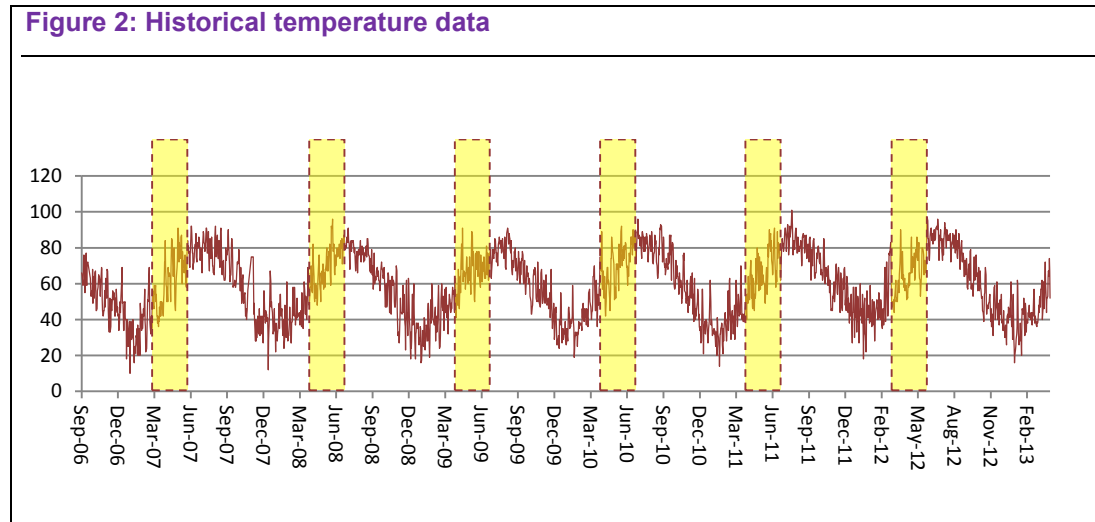
**Figure 1: Process for mapping heat index**

## Selecting Satellite Data

The Cambridge Study Area urban heat island was assessed by calculating land surface temperature from satellite data. Consistent with many thermal remote sensing studies (e.g., Rosenzweig et al., 2006; Kuscus and Sengezer, 2011; Rinner and Hussain, 2011), the heat island was characterized from one infrared image as opposed to averaging multiple images.

## Assessing Historical Data

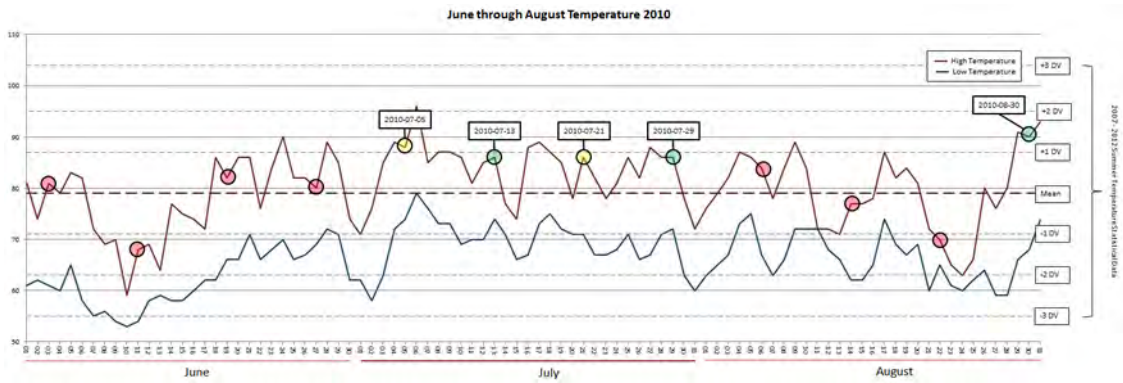
Daily maximum temperature measured at the MIT Green Building weather station between 2006 and present were imported into Excel. Summer (June through August) temperatures were assessed (Figure 2).



To guide satellite image selection, days when summer maximum temperatures were 1 or more standard deviations above mean summer temperature were identified. This criterion did not rely on consecutive days of elevated temperature, even though consecutive days of elevated temperature define heat waves. This discrepancy was intentional. Satellite data are typically only available during 2 or 3 days per month, and not all satellite data can be used for geospatial analyses, as cloud cover and other image quality issues can obscure land surface features. Due to the low temporal density of Landsat imagery, establishing criteria based on consecutive days of warm temperature would limit Landsat image assessment considerably, potentially ruling out images obtained when temperatures were warmer (Figure 3).



**Figure 3: Image availability, 2010**



Red dots indicate days when Landsat imagery is available, but temperatures are not 1 standard deviation above mean summer temperature.

Yellow dots indicate days when Landsat imagery is available and temperatures are at least 1 standard deviation above mean summer temperature, but fully processed products are not available.

Green dots indicate days when fully processed imagery is available and temperatures are at least 1 standard deviation above mean summer temperature.

For 2010, three Landsat images were downloaded based on image selection criteria.

## Downloading Satellite Data

Available Landsat data were assessed with the USGS Global Visualization Viewer (<http://glovis.usgs.gov/>). Images obtained during days when maximum temperatures were 1.5 or more standard deviations above mean summer temperature were visually assessed for cloud cover or other image quality issues impacting the Cambridge Study Area. Where image quality appears adequate for remote sensing, Landsat images were downloaded using the USGS Bulk Download Application ([http://earthexplorer.usgs.gov/resources/Bulk\\_tutorial\\_ee.pdf](http://earthexplorer.usgs.gov/resources/Bulk_tutorial_ee.pdf)).

## Selecting the Analysis Image

Downloaded Landsat data were loaded into GIS and further inspected visually. For the Cambridge Study Area, images suitable for remote sensing were all acquired from the Landsat 5 satellite. Therefore, digital numbers were all equally proportional to radiance, which is proportional to at-satellite temperature. This allowed relative temperature to be quickly assessed by comparing digital numbers in selected locations in each downloaded image. Digital numbers were compared at 10 locations. The image with the highest average digital numbers was also the image acquired during the day with the maximum historical temperature, August 30<sup>th</sup>, 2010.

## Converting Thermal Data to Radiance

The Landsat at-satellite radiance equation (equation 1) is published on the USGS Landsat website (USGS, 2013), the NASA Landsat 7 Science Users Handbook (NASA, 1998), and various Landsat- and thermal-remote-sensing-related publications (e.g., Chander et al., 2009; Xiong, 2012; Kuscü and Sengezer). While the equation for each Landsat product is the same, rescaling factors change. Rescaling factors can be obtained from Landsat metadata (USGS, 2013) or published literature (e.g., Chander et al., 2009).

## Converting Digital Numbers to Radiance

Landsat 5 thermal band digital numbers were converted to spectral radiance using the at-satellite radiance equation (equation 1). Rescaling factors were obtained from Chander and Markham (2003).

### Equation 1: Calculating thermal at-satellite spectral radiance

$$A_t - \text{Satellite Spectral Radiance} = G_{rescale} * Q_{cal} + B_{rescale}$$

Where:

$Q_{cal}$  is the satellite image pixel value, or digital number

$G_{rescale}$  is a band-specific rescaling factor (as published in Chander and Markham [2003]):  
 $0.055185 \text{ W/m}^2 * \text{sr} * \mu\text{m}$

$B_{rescale}$  is a band-specific rescaling factor (as published in Chander and Markham [2003]):  
 $1.2378 \text{ W/m}^2 * \text{sr} * \mu\text{m}$

## Estimating Emissivity

While at-satellite temperature can be calculated from at-satellite spectral radiance (equation 1), at-satellite temperature assumes uniform emissivity and a spectrally transparent atmosphere. To estimate land surface temperature, radiance should be corrected for emissivity variance (Section 3) and atmospheric distortion (Section 4) (Sobrino et al., 2004).

Emissivity describes radiation emission rates. Objects emit radiation at different rates. An emissivity of 1 indicates perfect emission. Lower values indicate slower rates. Because all objects obtain energy balance by warming until emitted energy equals absorbed energy, the slower the rate of emission, the warmer an object will become to reach balance. Instrumental, in situ measurements of emissivity are usually not available, so emissivity is typically estimated from satellite imagery (e.g., Sobrino et al, 2004).

Satellite-based estimates of emissivity often use the Normalized Difference Vegetation Index (NDVI) (e.g., Sobrino et al., 2004; Copertino et al., 2012; Liu and Zhang, 2011; Julien et al., 2011). NDVI is a vegetation index based on the proportion of reflected light in the visible red spectra (VIR, which plants absorb for photosynthesis) and reflected light in the near infrared spectra, (NIR, which plants usually do not absorb, as wavelengths are too long for photosynthesis). NDVI indicates relative vegetation density and health. Extensive research has consistently correlated NDVI with in situ, empirical datasets based on observations and measurements of vegetation, ecology, biology, and other related systems (Pettorelli, 2013). NDVI has been shown to be correlated with emissivity in multiple studies (e.g., Sobrino et al., 2004; Van, 1993).

To calculate NDVI, digital numbers must first be converted to at-satellite radiance (equation 2). At-satellite radiance is converted to reflectance, and NDVI is calculated from reflectance.

### Converting Digital Numbers to Radiance

Landsat 5 visible red (VIR, band 3) and near infrared (NIR, band 4) were converted to spectral radiance using the at-satellite radiance equation. Rescaling factors were obtained from Chander and Markham (2003) (equation 2).

#### Equation 2: Calculating VIR and NIR at-satellite spectral radiance

$$A_t - \text{Satellite Spectral Radiance} = G_{\text{rescale}} * Q_{\text{cal}} + B_{\text{rescale}}$$

Where:

$Q_{\text{cal}}$  is the satellite image pixel value, or digital number

$G_{\text{rescale}}$  is a band-specific rescaling factor (as published in Chander and Markham [2003]):

VIR:  $1.03988 \text{ W/m}^2 * \text{sr} * \mu\text{m}$

NIR:  $0.872588 \text{ W/m}^2 * \text{sr} * \mu\text{m}$

$B_{\text{rescale}}$  is a band-specific rescaling factor (as published in Chander and Markham [2003]):

VIR:  $-1.17 \text{ W/m}^2 * \text{sr} * \mu\text{m}$

NIR:  $-1.51 \text{ W/m}^2 * \text{sr} * \mu\text{m}$

### Converting Radiance to Atmosphere-corrected Reflectance

VIR and NIR spectral radiance (equation 2) was converted to atmosphere-corrected reflectance using equations 3, 4, and 5, as first published by Chavez (1996) and later adapted by Sobrino et al. (2004). The Chavez (1996) equations differ from those provided on the USGS website (USGS, 2011), because Chavez (1996) calculates the land surface reflectance by correcting for atmospheric distortion. VIR and NIR reflectance do not need to be corrected for emissivity,

because VIR and NIR reflectance is a measurement of solar energy reflected from the land surface rather than thermal energy radiated from the land surface.

**Equation 3: Calculating VIR and NIR atmosphere-corrected radiance**

$$Reflectance = \pi \frac{(L_{sat} - L_p)d^2}{E_0 \cos\theta_z T_z}$$

Where:

$L_{sat}$  is the spectral radiance (equation 2)

$T_z$  is the atmospheric transmittance (estimated from Chavez [1996] and Sobrino et al. [2004]):

VIR: 0.85

NIR: 0.91

$\theta_z$  is the Zenithal Solar Angle (from Landsat metadata):

VIR: 51.75083036

NIR: 51.75083036

$E_0$  is the spectral solar irradiance at the top of the atmosphere (Chander et al., 2009):

VIR: 1536

NIR: 1031

$d$  is the Earth-sun distance at the time the image was captured (Chander et al., 2009):

VIR: 1.00969

NIR: 1.00969

$L_p$  is the radiance resulting from interaction of electromagnetic radiance with atmospheric particles (calculated from Equation 4, after Chavez [1996] and Sobrino et al. [2004])

**Equation 4: Calculating  $L_p$  for equation 3**

$$L_p = L_{min} - L_{1\%}$$

Where:

$L_{min}$  is the radiance corresponding to the 0.01 percentile

VIR: 12.3484 (estimated from radiance histogram)

NIR: 6.34329 (estimated from radiance histogram)

$L_{1\%}$  is calculated from equation 5 (Sobrino et al., 2004):

#### Equation 5: Calculating $L_{1\%}$ for equation 4

$$L_{1\%} = \frac{0.01 \cos\theta_z T_z E_0}{\pi d^2}$$

Where:

$\theta_z$  is the Zenithal Solar Angle (from Landsat metadata):

VIR: 51.75083036

NIR: 51.75083036

$T_z$  is the atmospheric transmittance (estimated from Chavez [1996] and Sobrino et al. [2004]):

VIR: 0.85

NIR: 0.91

$E_0$  is the spectral solar irradiance at the top of the atmosphere (Chander et al., 2009):

VIR: 1536

NIR: 1031

$d$  is the Earth-sun distance at the time the image was captured (Chander et al., 2009):

VIR: 1.00969

NIR: 1.00969

## Calculating NDVI

NDVI was calculated from atmosphere-corrected reflectance (equations 3, 4, and 5) using equation 6 (Pettorelli, 2013; with Landsat 5 example Sobrino et al., 2004):

#### Equation 6: Calculating NDVI from NIR and VIR atmospherically-corrected reflectance

$$NDVI = \frac{NIR - VIR}{NIR + VIR}$$

Where:

NIR = Band 4 atmosphere-corrected reflectance (equations 3, 4, and 5)

VIR = Band 3 atmosphere-corrected reflectance (equations 3, 4, and 5)

## Estimating Emissivity from NDVI

Emissivity was estimated from NDVI using a modified (Sobrino et al., 2004) NDVI Thresholds Method (Van de Griend & Owe, 1993) (equations 7, 8, and 9). Similar NDVI-based emissivity estimates have been used in many thermal remote sensing studies (e.g., Sobrino et al., 2004; Liu and Zhang, 2011; Julien et al., 2011). The modified NDVI Thresholds Method in Sobrino et al.

(2004) was chosen because it has been tested against in situ emissivity measurements (Sobrino et al., 2004) and used in multiple subsequent thermal remote sensing studies (e.g., Copertino et al., 2012; Xiong et al., 2010).

#### Equation 7: Estimating emissivity from NDVI

$NDVI < 0.2$ :            *Bare Soil*  
 $NDVI > 0.5$ :            *Fully vegetated*  
 $NDVI \geq 0.2 \leq 0.5$ :    *Mixture of Soil and Vegetation*

##### Where

Bare Soil is 0.973, based on the mean soil emissivity in the ASTER soil spectral library calculated by Sobrino et al. (2004) and later applied by Copertino et al. [2012] and Xiong et al. [2010]

Fully vegetated is 0.999, based on typical vegetation emissivity assumed by Sobrino et al. (2004) and later assumed by Copertino et al. [2012] and Xiong et al. [2010]

Mixture of Soil and Vegetation is calculated from equation 8, after Sobrino et al. (2004) and later by Copertino et al. [2012] and Xiong et al. [2010]

#### Equation 8: Calculating soil/vegetation-mixture emissivity for equation 7

$$Emissivity = 0.004 P_v + 0.986$$

##### Where

$P_v$  is the vegetation proportion, calculated with equation 9, after Carson and Ripley (1997) and later by Sobrino et al. (2004), Copertino et al. (2012), and Xiong et al. (2010)

#### Equation 9: Calculating $P_v$ for equation 8

$$P_v = \left( \frac{NDVI - NDVI_{min}}{NDVI_{max} - NDVI_{min}} \right)^2$$

##### Where

$NDVI_{min}$  is 0.2, after Carson and Ripley (1997) and later by Sobrino et al. (2004), Copertino et al. (2012), and Xiong et al. (2010)

$NDVI_{max}$  is 0.5, after Carson and Ripley (1997) and later by Sobrino et al. (2004), Copertino et al. (2012), and Xiong et al. (2010)

## Estimating Atmospheric Distortion

Land surface temperature is calculated from radiance. At-satellite radiance (equation 1) can be calculated from digital numbers using rescaling factors. At-satellite radiance, however, is not a true measurement of land surface radiance. Thermal radiance is absorbed and scattered by the

atmosphere between the land surface where it is emitted and the satellite where it is sensed. Because less radiance is sensed by the satellite than was actually emitted at the land surface, calculating temperature from at-satellite radiance typically underestimates land surface temperature. To obtain accurate estimates of land surface temperature, atmospheric distortion should be corrected.

Multiple methods exist to estimate and correct for atmospheric distortion. Radiative transfer equations can be used to estimate land surface radiance. By obtaining an estimate of land surface radiance, land surface temperature can be estimated using an inverted Planck's Function (equations 12 and 13). Radiative transfer equations, however, require in situ or modeled atmospheric profile data. Because atmospheric profile data are often not available, other methods have been developed to estimate and correct for atmospheric distortion. Other methods typically use weather station measurements, assumptions of typical atmospheric conditions, and data readily available from satellite images to estimate the direct impact of the atmosphere on temperature. Because other methods estimate atmospheric impacts directly on temperature, one equation is used to estimate land surface temperature from at-satellite radiance and atmospheric parameters.

For the Cambridge Study Area, Land surface temperature was calculated using a radiative transfer equation. Atmospheric profile data were calculated using the NASA online MODTRAN tool. Radiative-transfer-equation-based methods based on modeled or in situ profiles tend to produce more accurate temperatures than other methods (e.g., Sobrino et al., 2004). Therefore, because atmospheric profile data were readily available for this study via the NASA online MODTRAN tool, a radiative transfer equation was used to correct temperature estimates for atmospheric distortion and emissivity.

### **NASA MODTRAN Tool**

Atmospheric parameters were estimated using the NASA online MODTRAN tool located at <http://atmcorr.gsfc.nasa.gov/> (Barsi et al., 2003). The online MODTRAN tool provides a modeled atmospheric profile for a given date, time, and location. It also provides three atmospheric parameters necessary for a simplified radiative transfer equation (equation 10): average atmospheric transmission, effective upwelling radiance, and effective downwelling radiance. In addition to date, time, and location, the user can provide altitude, temperature, pressure, and relative humidity to better constrain model results.

## Parameter Selection

The online MODTRAN tool was used to estimate atmospheric transmission, upwelling radiance, and downwelling radiance at the MIT Green Building weather station (Lat: 42.360, Long: -71.089) at the date and time the satellite data used in this study were captured (2010-08-30 at 15:17 GMT). The MIT weather station location was used due to the availability of empirical station data for constraining and back checking model results. The mid-latitude summer standard profile was selected, and the atmospheric profile was based on the Landsat-5 band-6 spectral curve, because this study uses Landsat-5 band-6 data.

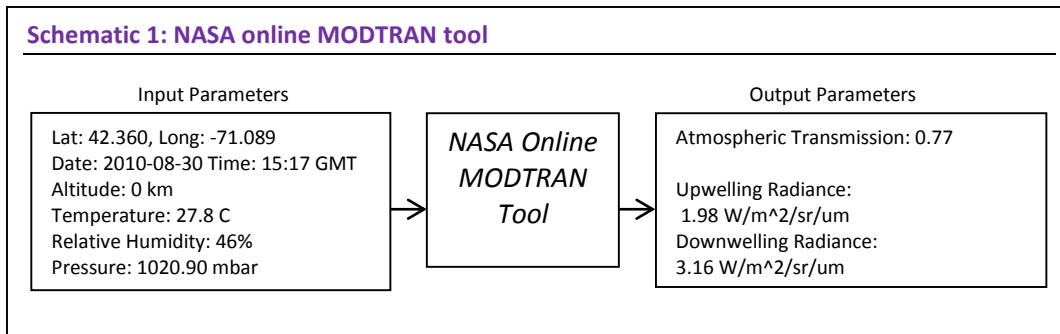
Model sensitivity to altitude, temperature, relative humidity, and pressure was tested prior to final parameter selection. Changing these parameters from default (not provided; model-based) to values measured at the Cambridge weather station did not change results considerably, and it appeared the MIT Green Building altitude was within the modeled-altitude margin of error. Vertical resolution in modeled atmospheric profile data was too coarse for precise comparison with MIT station data. Moreover, attempts to model the atmospheric profile at the MIT Green Building weather station altitude (about 20 meters) resulted in atmospheric curves starting at the MIT Green Building weather station altitude rather than the ground surface (about 6 meters), though this difference may have been due to vertical resolution in the atmospheric profile.

Based on sensitivity analyses, the typical Cambridge elevation (6 meters) rounded to the nearest hundredth of a kilometer (0 kilometers) was used, and surface pressure (1020.90 mbar), temperature (~27.8 C), and relative humidity (46%) were selected based on Cambridge station measurements and the resulting atmospheric profile, which was generally consistent with known Cambridge measurements.

## Model Output

Selected parameters resulted in an atmospheric transmission of 0.77, upwelling radiance of 1.98  $W/m^2/sr/\mu m$ , and downwelling radiance of 3.16  $W/m^2/sr/\mu m$ . Atmospheric transmission remained a constant 0.77 in sensitivity analyses, while upwelling radiance varied from 1.92 to 1.99  $W/m^2/sr/\mu m$  and downwelling radiance varied from 3.06 to 3.17  $W/m^2/sr/\mu m$ .





## Calculating Emissivity- and Atmosphere-corrected Land Surface Temperature

Atmospheric distortion and emissivity were corrected via a radiative transfer equation (equation 10). The radiative transfer equation relies on a modeled atmospheric profile (schematic 1) to estimate atmospheric transmission (schematic 1), upwelling radiance (schematic 1), and downwelling radiance (schematic 1). The radiative transfer equation also corrects radiance for land surface emissivity, which was estimated in equations 7, 8, and 9.

Planck's Function (equation 11) was used to calculate temperature from corrected land surface radiance. Planck's function relates spectral intensity (radiance) with wavelength and temperature. By inverting Planck's Function (solving for temperature, equation 12), temperature can be calculated using radiance and Landsat constants provided by the USGS website (USGS, 2011), Landsat 7 Science User Guide Handbook (NASA, 1998), and numerous publications (e.g., Chander et al., 2009; Xiong et al., 2012; Coll et al., 2010; Kuscu and Sengezer, 2011)

### Correcting Radiance

Radiance was corrected for atmospheric distortion and land surface emissivity via a radiative transfer equation (equation 10) (e.g., Coll et al., 2010; Kuscu and Sengezer, 2011). The radiative transfer equation uses at-satellite radiance (equation 1), land surface emissivity (equations 7, 8, and 9), atmospheric transmission (schematic 1), upwelling radiance (schematic 1), and downwelling radiance (schematic 1) to estimate the ground surface radiance.

#### Equation 10: Estimating land surface radiance via a simplified radiative equation

$$\text{land surface radiance} = \frac{L_{\text{sen}} - L_{\uparrow}}{\varepsilon T} - \frac{1 - \varepsilon}{\varepsilon} L_{\downarrow}$$

Where

$L_{\text{sen}}$  is the at-satellite radiance (equation 1)

$L_{\uparrow}$  is the upwelling radiance (schematic 1)

$L_{\downarrow}$  is the downwelling radiance (schematic 1)

$\varepsilon$  is the emissivity (equations 7, 8, and 9)

$T$  is the mean atmospheric transmission (schematic 1)

### Calculating Land Surface Temperature

Land surface temperature was calculated from the Landsat 5 Planck's Inversion (equation 12) using atmosphere- and emissivity-corrected radiance (equation 10). Land surface temperature is calculated in degrees kelvin. Temperature was converted to degrees Fahrenheit for this study (equation not shown).

Planck's law relates the spectral intensity of radiation with wavelength and temperature:

#### Equation 11: Planck's Function: Spectral Intensity from Wavelength and Temperature

$$B\lambda(T) = \frac{2hc^2\lambda^{-5}}{e^{hc/k\lambda T} - 1}$$

Where

$B\lambda(T)$  is the spectral intensity at a given temperature

$h$  is Planck's constant ( $6.626068 \times 10^{-27}$  erg sec)

$c$  is the speed of light in a vacuum ( $2.997925 \times 10^{10}$  cm/sec)

$k$  is Boltzman's Constant ( $1.38066 \times 10^{-16}$  erg deg<sup>-1</sup>)

$\lambda$  is the wavelength

$T$  is the temperature in kelvin

By inverting Planck's Function (solving for temperature), brightness temperature can be obtained from spectral intensity (radiance) and wavelength:

### Equation 12: Inverting Planck's Function

$$B\lambda(T) = \frac{2hc^2\lambda^{-5}}{e^{hc/k\lambda T} - 1}$$

therefore

$$e^{hc/k\lambda T} - 1 = \frac{2hc^2\lambda^{-5}}{B\lambda(T)}$$

therefore

$$\frac{hc}{K\lambda T} = \ln\left(\frac{2hc^2\lambda^{-5}}{B\lambda(T)}\right) + 1$$

therefore

$$T = \left(\frac{hc}{K\lambda}\right) \frac{1}{\left(\ln\left(\frac{2hc^2\lambda^{-5}}{B\lambda(T)}\right) + 1\right)}$$

Landsat provides numerical values for terms  $2hc^2\lambda^{-5}$  and  $\frac{hc}{K\lambda}$  as constants K1 and K2. These constants are provided by the USGS Landsat website (USGS, 2011), the Landsat 7 Science User Handbook (NASA, 1998), and later defined in Chander et al. (2003) and republished in numerous publications (e.g., Kuscü and Sengezer, 2011; Chen et al., 2005). These constants are applied to the inverted Planck Function (equation 12) to obtain the brightness temperature equation for Landsat 5 (Equation 13). Note that, aside from radiance, remaining terms are unitless. Constants K1 and K2 are provided with units consistent with calculated radiance (equations 1 and 10). Therefore, no units require conversion.

### Equation 13: Landsat 5 Brightness Temperature Equation

$$\text{Temperature (kelvin)} = \frac{K2}{\ln\left(\frac{K1}{L\lambda} + 1\right)}$$

Where:

K1 is a calibration constant 1 (607.76 W/m<sup>2</sup> \* sr \* μm)

K2 is a calibration constant 2 (1260.56 kelvin)

Lλ is Spectral Radiance

## Estimating Ambient Air Temperature

Land surface temperature is typically warmer than the ambient air temperature that is measured by weather stations and felt by humans. Therefore, land surface temperature was adjusted to estimate ambient air temperature.

## Adjusting Land Surface Temperature

To estimate ambient air temperature, a regression model was adapted from Kloog et al. (2014). The model was developed from correlations developed in the general Cambridge study area between land surface temperature, ambient air surface temperature as measured by weather stations, elevation, NDVI, and percent urban as calculated from the National Land Cover Database (equation 14):

### Equation 14: Average ambient air vs land surface temperature ratio

$$\text{Ambient Air Temperature} = (M1 * LST) + (M2 * \text{Percent Urban}) + (M3 * \text{Elevation}) + (M4 * NDVI) + B$$

Where

M1 is the LST slope, 0.38

(To calibrate the model, M1 was calculated only from Cambridge and nearby Stations)

M2 is the sum of the fixed and random Percent Urban slopes, -0.00124972102607794

M3 is the sum of the fixed and random elevation slopes, -0.000961258057526494

M4 is the sum of the fixed and random NDVI slopes, -1.333087855

LST is the LST from equation 13

Percent Urban is calculated from the mean value of NLCD Percent Urban Categorizations

Elevation is calculated from LiDAR

NDVI is the NDVI calculated from equation 6

B is the sum of the fixed and random intercepts, 14.8171859697681

Estimated ambient air temperatures were compared with measured ambient air temperatures at the two available Cambridge weather stations.

Station	Measured Ambient Air Temperature	Calculated Ambient Temperature
KMACAMBR9	81.8	81.2
KMACAMBR4	85.7	89.8

The KMACAMBR9 temperature is accurate to within 1 degree F, while the KMACAMBR4 temperature is accurate to within about 4 degrees F. These two stations indicate an average accuracy to within about 2.5 degrees F; however, this comparison is limited due to small sample size. Estimated ambient air temperature is depicted on Figure 4 below.

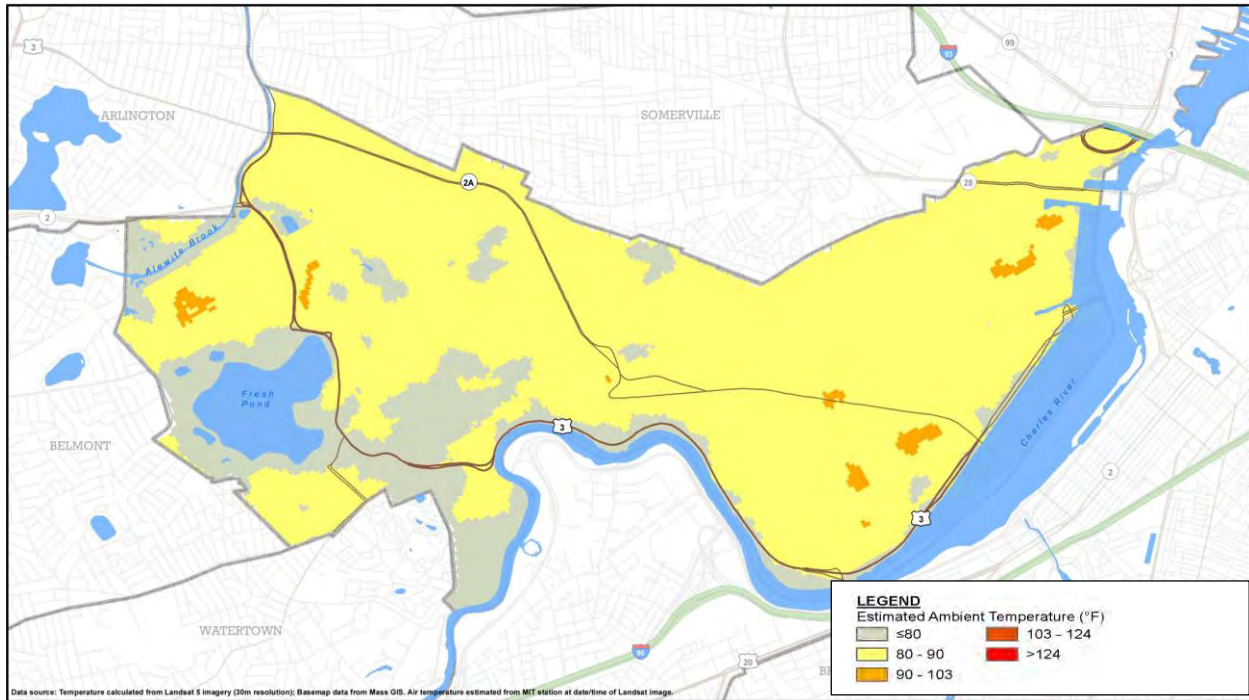


Figure 4: Estimated existing ambient air temperature (Kleinfelder, November 2015)

## Calculating Heat Index

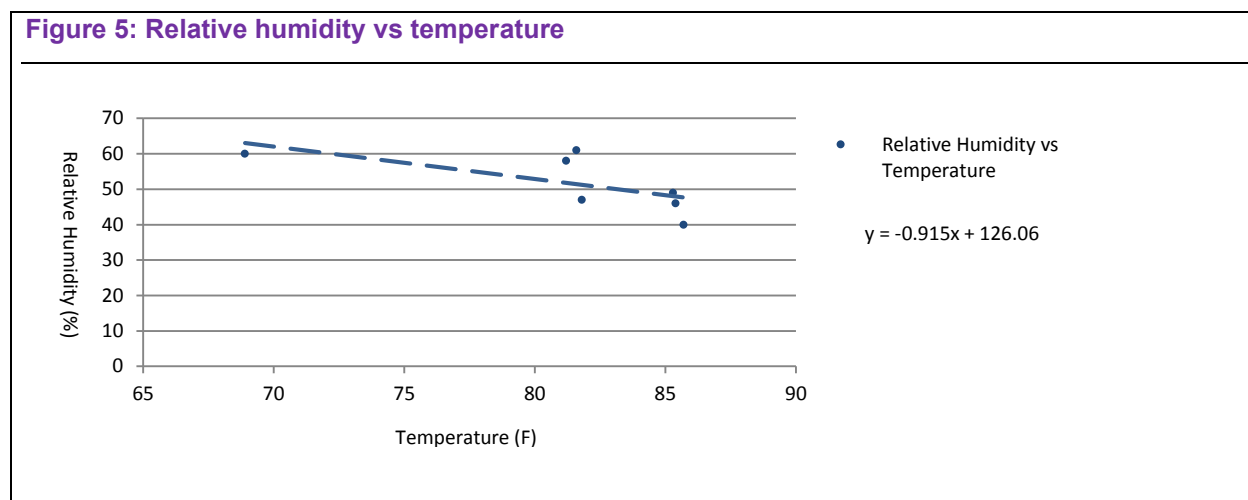
Heat index is a measurement of how temperature feels to humans. Heat index was calculated with the standard NOAA regression, which relates average heat index to ambient air temperature and relative humidity (equation 16). Since relative humidity is used to calculate heat index, relative humidity was estimated.

## Estimating Relative Humidity

As a first approximation, heat index was first calculated using the relative humidity measured at the MIT weather station. Using this constant relative humidity for each pixel-calculated ambient air temperature resulted in heat indices sometimes exceeding 130. These results did not appear

realistic, as they would predict heat-related health issues, which do not appear to have occurred when these Landsat 5 data were captured. Therefore, relative humidity was assessed further.

Because relative humidity is generally inversely proportional to temperature (e.g., Souch and Souch, 1993), relative humidity and temperature data from the same date and time were gathered from nearby weather stations. Relative humidity ranged from 40% to 61%. Data were plotted in Excel and a linear regression was calculated (Figure 5).



This relationship was investigated further over longer timescales. Longer timescales increased sample size, and a relationship was still evident with increased sample size; however, the slope of the regression was found to be temporally-sensitive. Therefore, a simple linear regression model based on temperature and relative humidity data from the same date and time that the Landsat data were captured was used to estimate relative humidity (equation 15):

**Equation 15: Estimating relative humidity from ambient air temperature**

$$\text{Relative Humidity} = -0.915t + 126.06$$

Where  
t is the ambient air temperature (equation 14)

### Calculating Heat Index

Heat index was calculated using the standard NOAA equation (equation 16), which relates heat index to temperature and relative humidity. This is the standard equation used for the NOAA heat index calculator (NOAA, 2013). This heat index equation was derived from a multiple regression

analysis of numerous variables used to model heat index. The goal of the regression was to create a practical way for forecasting heat index from conventional variables (i.e., temperature and relative humidity) (Rothfusz, 1990):

**Equation 7.2.1: Calculating heat index**

$$\begin{aligned} \text{Heat index} = & -42.379 + 2.04901523 * T + 10.14333127 * RH - .22475541 * T * \\ & RH - .00683783 * T * T - .05481717 * RH * RH + .00122874 * T * T * RH + \\ & .00085282 * T * RH * RH - .00000199 * T * T * RH * RH \end{aligned}$$

*Where*

T is the ambient air temperature (equation 14)

RH is the relative humidity (equation 15)

Special adjustments are required where relative humidity is less than 13% and temperature is between 80 and 112 °F. These conditions were not encountered in the Cambridge Study Area. Special adjustments are also required where relative humidity is greater than 85% and temperature is between 80 and 87 °F. Again, these conditions were not encountered in the Cambridge Study Area. Finally, the heat index equation is considered invalid where heat index is less than 80. Where it is less than 80, a simplified regression is used (equation 17). Heat index was therefore recalculated as per equation 17 where heat index was less than 80. Estimated heat index is depicted on Figure 6.

**Equation 17: Calculating heat index where heat index is less than 80**

$$\text{Heat index} = 0.5 * (T + 61.0 + ((T - 68.0) * 1.2) + RH * 0.094))$$

*Where*

T is the ambient air temperature (equation 14)

RH is the relative humidity (equation 15)

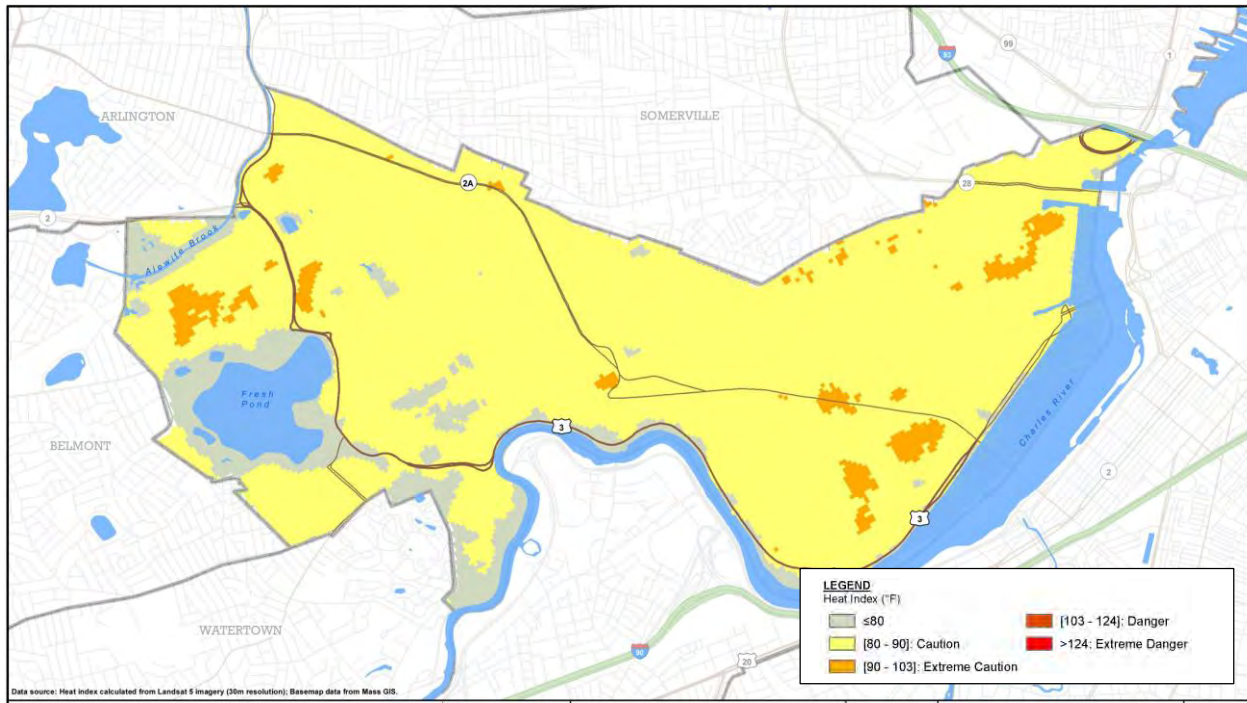


**Figure 6: Estimated existing heat index.** The colors used to represent heat index are based on the colors used for the NOAA heat index chart (Kleinfelder, November 2015)

## Estimating the Cooling Impact of Vegetation

Numerous studies have indicated a direct, casual relationship between vegetation and temperature. It is well established that increased vegetation decreases temperature. This relationship is often identified as one of the largest contributors to temperature variance over localized areas (e.g., Rosenzweig et al. 2008; Ogashawara and Bastos, 2012; Rinner and Hussain, 2011). The impact of tree canopy (the layer of branches and leaves that shade the land surface) is even higher, as tree canopy can absorb 70 to 90% of incoming solar radiation (EPA, 2008).

Trees are commonly planted to mitigate heat islands. Therefore, future conditions heat island projections may be altered considerably based on current and future tree planting. If numerous trees are planted in areas most susceptible to the heat island effect, future temperatures in susceptible areas may decrease considerably compared with future condition projections based on currently existing tree canopy (EPA, 2008).

The potential cooling effect of tree planting can be estimated by investigating the spatial relationship between existing-conditions temperature and tree canopy. Because a significant, causal relationship between temperature and trees is well established, the spatial correlation



between temperature and tree canopy can be used to estimate the cooling impact of trees to a first approximation. This first approximation can be improved by considering other factors that influence temperature, including impervious surfaces, bare areas, and other urban infrastructure.

### Estimating Tree Canopy

Tree canopy data were obtained from the University of Vermont (O’Neil-Dunne, 2012). O’Neil-Dunne (2012) used LiDAR data and high-resolution satellite imagery to assess the Cambridge tree canopy. A 250-foot-wide grid network, or fishnet, was created, and tree canopy percentage per grid was calculated.

### Calculating Average Temperature

To compare tree canopy percentage with temperature, existing tree canopy data were down-sampled and existing tree canopy percentage per ambient air temperature grid was calculated using ArcGIS zonal statistics (Figure 7). Grids overlaying water bodies were removed to decrease cooling bias due to water. All data were stored in a shapefile for easy import into Excel.

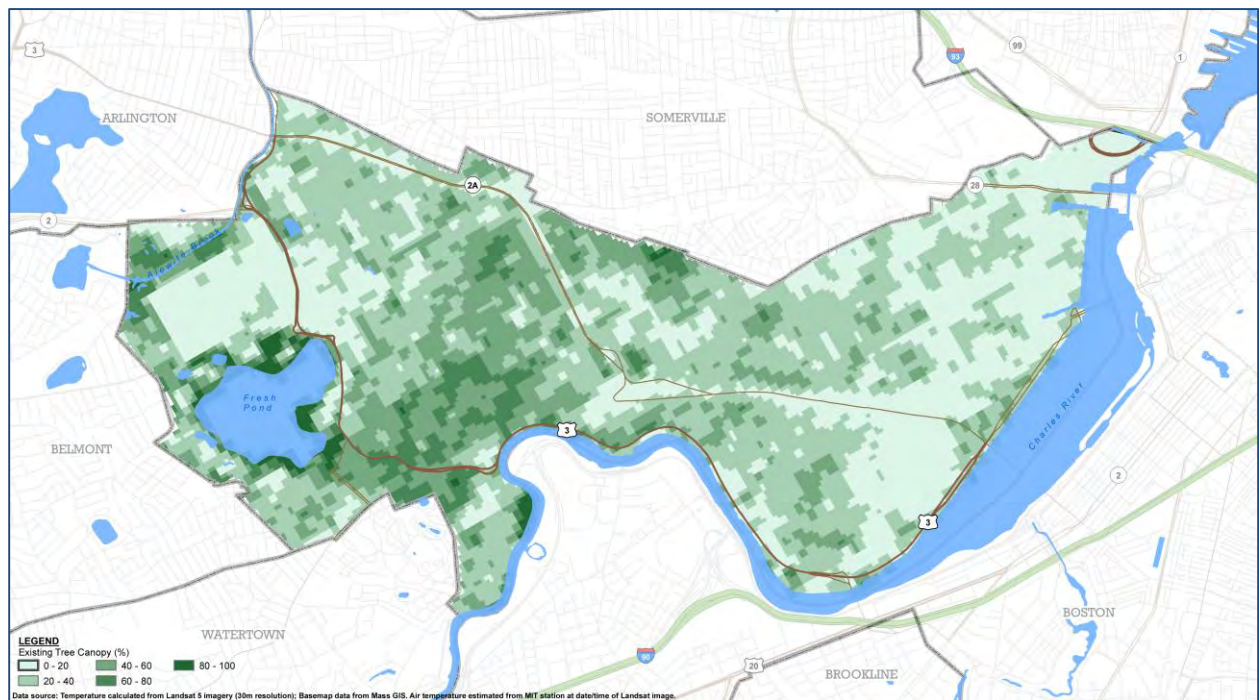


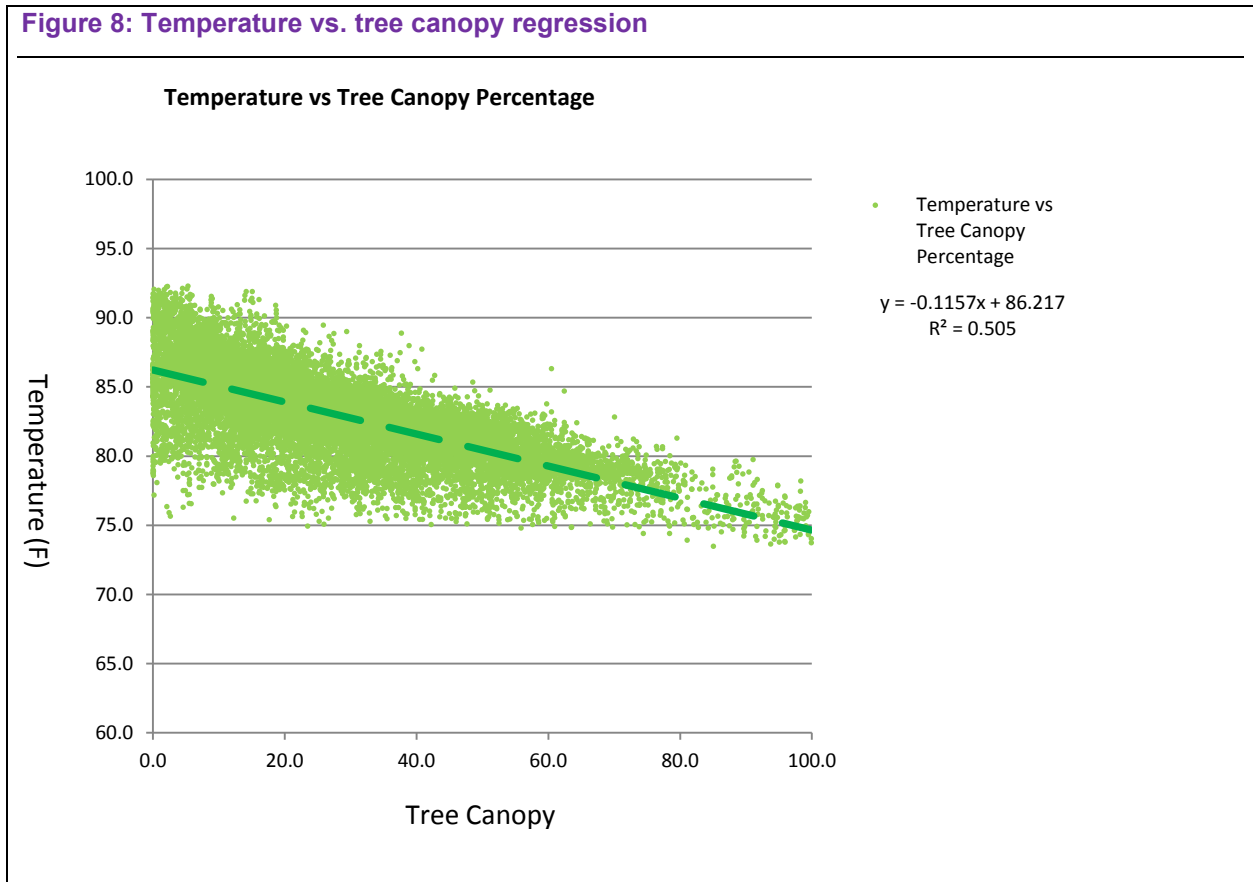
Figure 7: Existing tree canopy (Source: Kleinfelder using U. Vermont database, November 2015)

### Analyzing Temperature and Tree Canopy Data

Tree canopy percentage and temperature data were imported into Excel for analysis. Temperature was plotted against tree canopy, and a simple linear regression was calculated

relating temperature with tree canopy percentage (Figure 8, equation 18). The  $R^2$  for this regression is about 0.44, which indicates that tree canopy percentage alone explains almost half the variance in temperature distribution.

**Figure 8: Temperature vs. tree canopy regression**



**Equation 18: Temperature vs. tree canopy regression**

$$\text{temperature} = -0.1157tc + 82.217$$

Where

tc is tree canopy percentage

### Estimating the Cooling Impact of Vegetation

Equation 18 was used to estimate the cooling impact of vegetation. The slope of the regression (-0.1157) indicates that, at first approximation, each percent increase in tree canopy decreases temperature by about 0.12 °F. Therefore, tree canopy percentage was multiplied by the regression slope (equation 19) to estimate its cooling impact.

**Equation 19: Estimating Cooling Impact of Tree Canopy**

$$\text{Cooling } (^{\circ}\text{F}) = -0.1157tc$$

*Where*

tc is tree canopy percentage

The estimated cooling impact of tree canopy is depicted on Figure 9. The  $R^2$  of about 0.5 indicates that about half the variation in temperature is mathematically explained by tree canopy. A more advanced model considering other variables known to impact temperature may improve the  $R^2$ . The single variable analysis (equation 19), however, indicates the highest percentage of tree canopy (between 80 to 100%) is consistently correlated with the lowest temperatures (about 75 to 80 °F), whereas lower percentages of tree canopy (0 to 80%) are usually correlated with higher temperatures, but not nearly so consistently (temperatures are usually 80 to 90 °F, but are sometimes as low as 75 °F). In other words, temperature variance increases with decreased tree canopy percent. This indicates that under maximum tree canopy conditions, the impacts of other factors are diminished. While variance in the highest temperatures may be better explained with a combination of tree canopy and other factors that cause additional warming, other factors appear to have little impact when tree canopy is maximized, as indicated by decreased temperature variance under maximum tree canopy. When maximized, the cooling impact of tree canopy appears to overwhelm other factors. For this reason, the regression slope of -0.1157 was used to estimate cooling impact of vegetation at a first approximation, despite the  $R^2$  of 0.505.

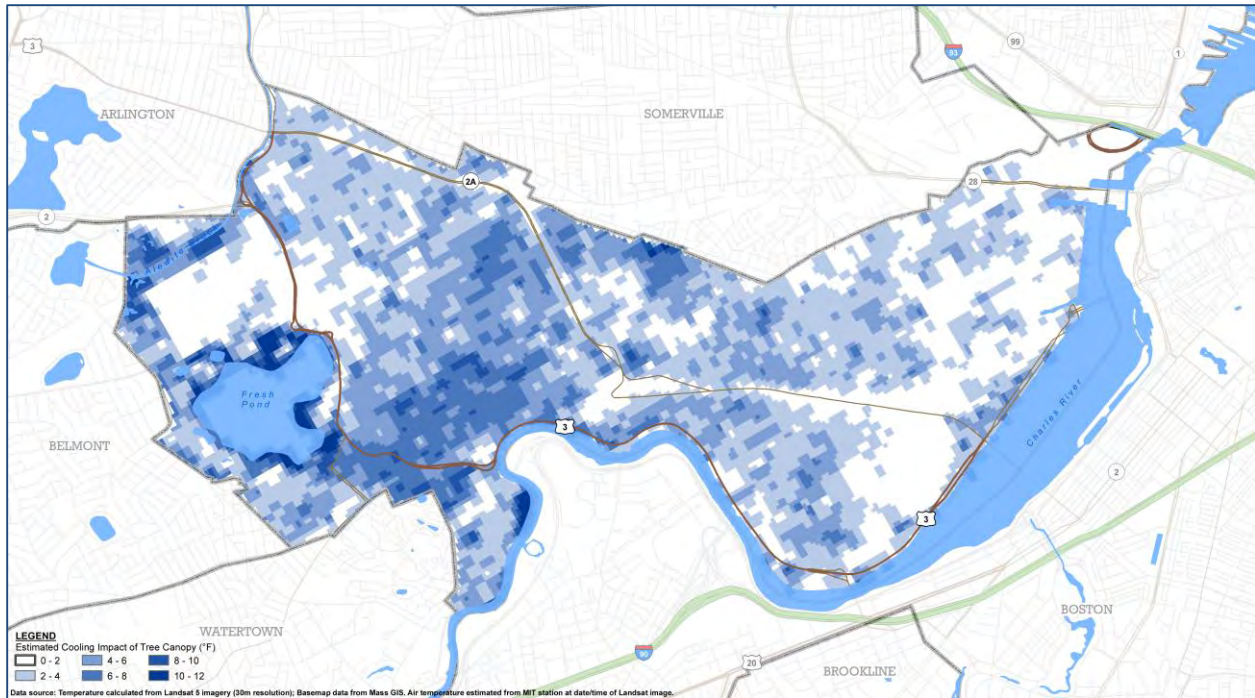


**Figure 9: Mapping estimated cooling impact of tree canopy (Kleinfelder, November 2015)**

## Future Conditions

Ambient air temperature variability due to urban heat island effect in the future was estimated based on the ratio between average ambient air temperature for existing conditions and average ambient air temperature for projected future scenarios. Heat index variability was estimated based on the ratio between average heat index for existing conditions and average heat index for projected future scenarios. Existing conditions were based on Cambridge weather station measurements taken at the same time and date as the Cambridge heat island. Future conditions were based on likely future scenarios of ambient temperature and heat index. These scenarios were selected based on a combination of historic extreme heat events experienced in the City of Cambridge, and downscaled climate change projections for the City

### Estimating Future Conditions of Ambient Air Temperature

Future conditions of ambient air temperature variability for 2030s (Figure 10) and 2070s (Figure 11) for Cambridge was estimated by considering separate scenarios for 2030s and 2070s. For 2030s, the scenario selected was four consecutive days with ambient air temperature at 90°F day. For 2070s, the scenario selected was five consecutive days with ambient air temperature greater than or equal to 90°F, including three days at 100°F. Therefore, equation 20 was applied to each existing-conditions ambient-air-temperature raster cell to estimate future ambient air

temperature in Cambridge by the 2030s, and equation 21 was applied to each existing-conditions ambient-air-temperature raster cell to estimate future ambient air temperature by the 2070s.

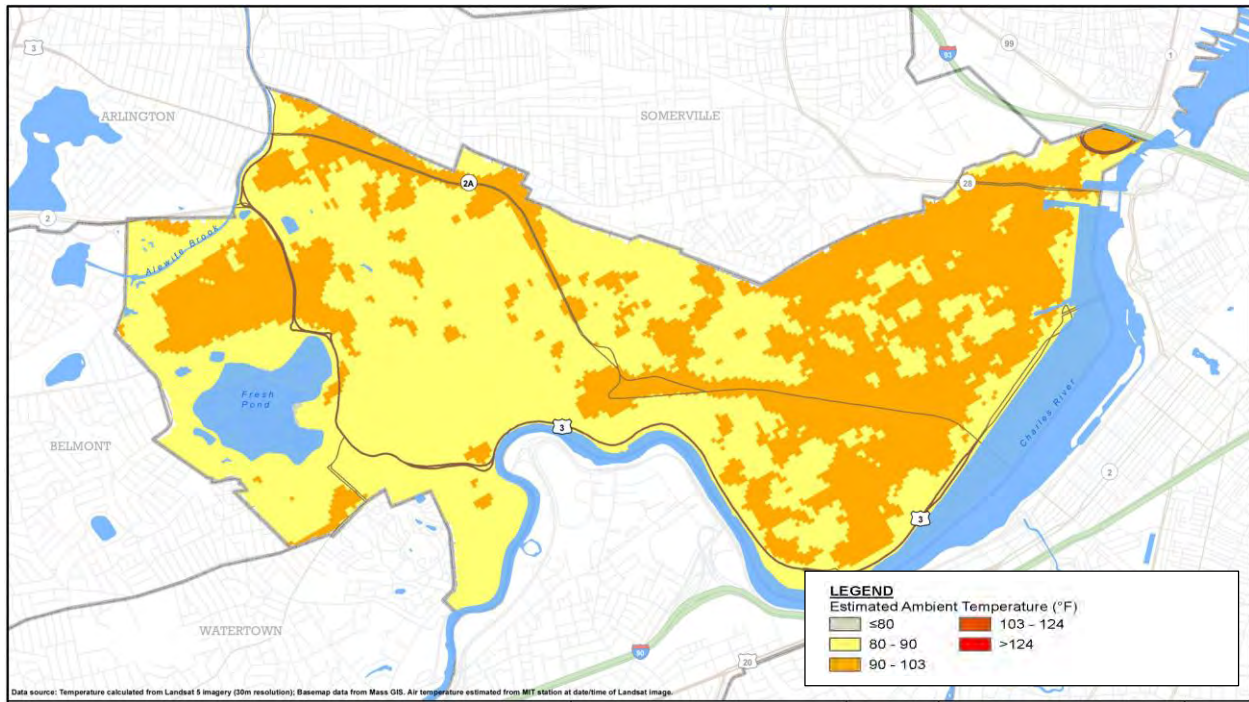


Figure 10: Estimated future conditions ambient air temperature variability for 2030s (November 2015)

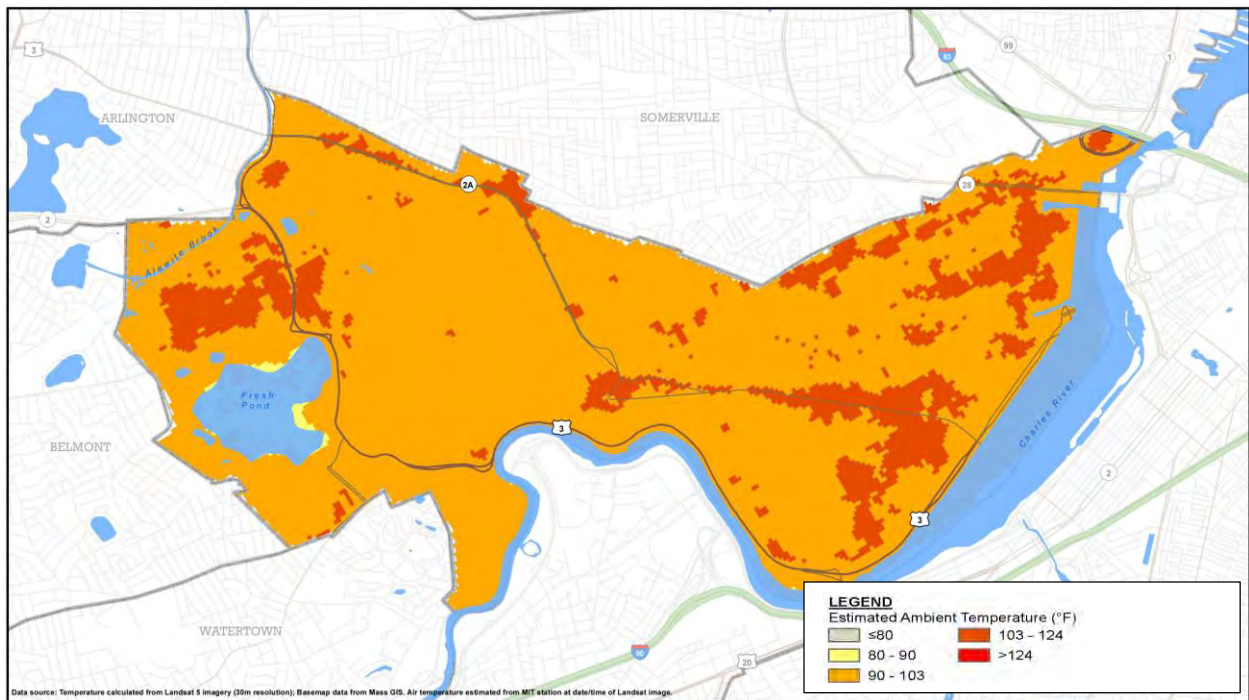


Figure 11: Estimated future conditions ambient air temperature variability for 2070s (November 2015)

**Equation 20: Future conditions ambient air temperature for 2030**

$$\text{Projected Air Temperature for 2030s} = \left( \frac{\text{Average Temperature for Projected 2030s Scenario}}{\text{Average Temperature for Existing Conditions}} \right) * \text{Existing Temperature}$$

*Where*

Existing temperature is the estimated ambient air temperature from equation 14

Future conditions is 90°F, from the 2030s scenario

Existing conditions is 83.3°F, from average ambient air measured in Cambridge weather stations

**Equation 21: Future conditions ambient air temperature for 2070**

$$\text{Projected Air Temperature for 2070s} = \left( \frac{\text{Average Temperature for Projected 2070s Scenario}}{\text{Average Temperature for Existing Conditions}} \right) * \text{Existing Temperature}$$

*Where*

Existing temperature is the estimated ambient air temperature from equation 14

Future conditions is 100°F, from the 2070s scenario

Existing conditions is 83.3°F, from average ambient air measured in Cambridge weather stations

**Estimating Future Conditions Heat Index**

Future conditions heat index variability for 2030s (Figure 12) and 2070s (Figure 13) for Cambridge was estimated by considering separate scenarios for 2030s and 2070s. For 2030s, the scenario selected was four consecutive days with heat index at 96°F. For 2070s, the scenario selected was five consecutive days with heat index greater than or equal to 110°F (ambient air temperature of about 90°F with 60 to 65% relative humidity), including three days at 115 °F. Therefore, Equation 22 was applied to each existing-conditions heat-index raster cell to estimate future heat index in Cambridge by the 2030s, and Equation 23 was applied to each existing-conditions heat index raster cell to estimate future heat index by the 2070s.

**Equation 22: Future conditions heat index for 2030**

$$\text{Projected Heat Index for 2030s} = \left( \frac{\text{Average Heat Index for Projected 2030s Scenario}}{\text{Average Heat Index for Existing Conditions}} \right) * \text{Existing Temperature}$$

*Existing Temperature*

*Where*

Existing temperature is the estimated ambient air temperature from equation 16

Future conditions is 96°F, from the 2030s scenario

Existing conditions is 84.1°F, from average ambient air measured in Cambridge weather stations

**Equation 23: Future conditions heat index for 2070**

$$\text{Projected Heat Index for 2070s} = \left( \frac{\text{Average Heat Index for Projected 2070s Scenario}}{\text{Average Heat Index for Existing Conditions}} \right) * \text{Existing Temperature}$$

*Existing Temperature*

*Where*

Existing temperature is the estimated ambient air temperature from equation 16

Future conditions is 115°F, from the 2070s scenario

Existing conditions is 84.1°F, from average ambient air measured in Cambridge weather stations

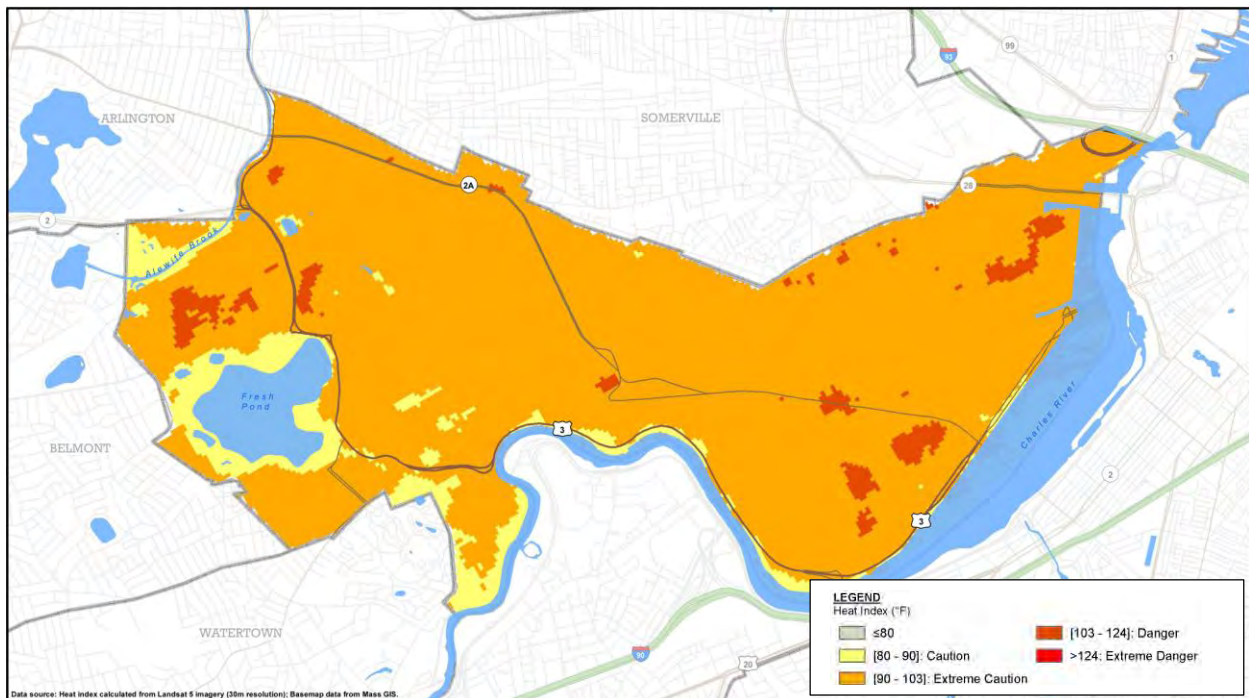


**Figure 12: Future conditions heat index variability for 2030s (November 2015)**

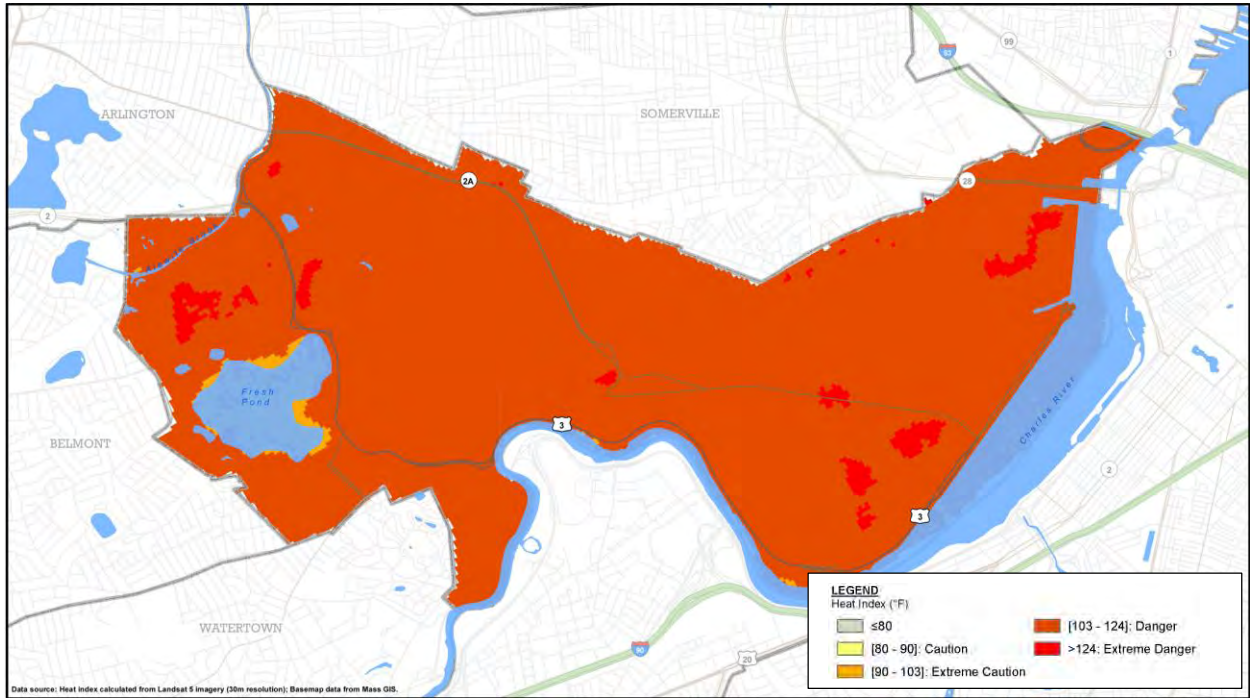


Figure 13: Future conditions heat index variability for 2070s (November 2015)



## References

- Barsi et al., 2003, An Atmospheric Correction Parameter Calculator for a Single Thermal Band Earth-Sensing Instrument, IEEE Geoscience and Remote Sensing Symposium, Volume 5, pages 3014-3016
- Chander and Markham, 2003, Revised Landsat-5 TM Radiometric Calibration Procedures and Postcalibration Dynamic Ranges, IEEE Transactions on Geoscience and Remote Sensing, Volume 41, pages 2674-2677
- Chander et al., 2009, Summary of Current Radiometric Calibration Coefficients for Landsat MSS, TM, ETM+, and EO-1 ALI Sensors, Remote Sensing of Environment, Volume 113, pages 893-903
- Coll et al., 2010, Validation of Landsat-7 ETM+ Thermal-Band Calibration and Atmospheric Correction With Ground-Based Measurements, IEEE Transactions on Geoscience and Remote Sensing, Volume 48, Number 1, pages 547 – 555
- Copertino et al., 2012, Comparison of Algorithms to Retrieve Land Surface Temperature from LANDSAT-7 ETM+ IR Data in the Basilicata Ionian Band, Tethys, Vol. 9, pages 25-34
- EPA, 2008, Reducing Urban Heat Island: Compendium of Strategies – Heat Island Basics
- Julien et al., 2011, Temporal Analysis of Normalized Difference Vegetation Index (NDVI) and Land Surface Temperature (LST) Parameters to Detect Changes in the Iberian Land Cover Between 1981 and 2001, International Journal of Remote Sensing, Volume 32, pages 2057-2068
- Kloog et al., 2014, Predicting Spatiotemporal Mean Air Temperature Using MODIS Satellite Surface Temperature Measurements across the Northeastern USA, Remote Sensing of Environment, Volume 150, pages 132-139
- Kuscu and Sengezer, 2011, Determination of Heat Islands from Landsat Tm Data: Relationship between Surface Temperature and Urbanization Factors in Istanbul, 34th International Symposium on Remote Sensing of Environment
- Liu and Zhang, 2011, Urban Heat Island Analysis Using the Landsat TM Data and ASTER Data; A Case Study in Hong Kong, Remote Sensing, Volume 3, pages 1535-1552
- NASA, 1998, Landsat 7 science data users' handbook
- O'Neil-Dunne, 2012, A Report on the City of Cambridge's Existing and Possible Tree Canopy

Ogashawara and Bastos, 2012, A Quantitative Approach for Analyzing the Relationship between Urban Heat Islands and Land Cover, *Remote Sensing*, Volume 4, pages 3596-3618

Pettorelli, 2013, *The Normalized Difference Vegetation Index*, Oxford University Press

Rinner and Hussain, 2011, Toronto's Urban Heat Island—Exploring the Relationship between Land use and Temperature, *Remote Sensing*

Rosenzweig et al., 2006, Mitigating New York City's Heat Island With Urban Forestry, Living Roofs, and Light Surfaces, *The International Archives of Photogrammetry, Remote Sensing and Spatial Information Sciences*, Vol. XXXVIII-4/C7

Rothfus, 1990, The Heat Index "Equation" (or, More Than You Ever Wanted to Know About Heat Index), NOAA Technical Attachment SR 90-23

Sobrino, 2004, Land Surface Temperature Retrieval from Landsat TM 5, *Remote Sensing of Environment*

Souch and Souch, 1993, The Effect of Trees on Summertime Below Canopy Urban Climates: A Case Study Bloomington, Indiana, *Journal of Arboriculture*, 19(5), pages 303-312

USGS, 2013, [http://landsat.usgs.gov/how\\_is\\_radiance\\_calculated.php](http://landsat.usgs.gov/how_is_radiance_calculated.php)

Van de Griend & Owe, 1993, On the Relationship Between Thermal Emissivity and the Normalized Difference Vegetation Index for Natural Surfaces, *International Journal of Remote Sensing*, 14(6), pages 1119–1131.

Xiong, 2012, The Impacts of Rapid Urbanization on the Thermal Environment; A Remote Sensing Study of Guangzhou, South China, *Remote Sensing*, Volume 4, pages 2033-2056